


Anticorrelation in nonsequential double ionization of helium

Zhangjin Chen  and Anran Zhou 

Department of Physics, College of Science, Shantou University, Shantou, Guangdong 515063, People's Republic of China

Toru Morishita

Institute for Advanced Science, The University of Electro-Communications, 1-5-1 Chofu-ga-oka, Chofu-shi, Tokyo 182-8585, Japan

Yuxing Bai  and Xiaolei Hao

Institute of Theoretical Physics and Department of Physics, Shanxi University, Taiyuan 030006, People's Republic of China

Oleg Zatsarinny and Klaus Bartschat

Department of Physics and Astronomy, Drake University, Des Moines, Iowa 50311, USA



(Received 19 February 2021; accepted 21 April 2021; published 4 May 2021)

We calculate the correlated two-electron momentum distributions for nonsequential double ionization of helium in a 400-nm laser pulse with a peak intensity of 6.5×10^{14} W/cm², which is below the recollision threshold, by using the quantitative rescattering model in which the lowering of the threshold due to the presence of the electric field at the instant of recollision is taken into account. While distinct correlated back-to-back emission of the electrons along the polarization direction is predicted in accord with other existing theoretical simulations, we suggest an alternative mechanism that is responsible for the anticorrelation. At intensities below the recollision threshold, recollision excitation can only take place when the barrier of the Coulomb potential is sufficiently suppressed by the electric field. The excited electron begins to ionize at a “delayed” recollision time after a crossing of the field and hence the probability of being tunnel-ionized after the subsequent peak of the field is increased. It is demonstrated that the “delayed” recollision time predominantly determines the parallel momentum distribution of the tunneling electron and plays a decisive role in forming anticorrelation.

DOI: [10.1103/PhysRevA.103.053102](https://doi.org/10.1103/PhysRevA.103.053102)

I. INTRODUCTION

It has been well established that nonsequential double ionization (NSDI) is a laser-induced recollision process that can be interpreted by the classical rescattering model [1,2]. In the rescattering picture, one electron is first released through quantum tunneling, then it is driven back by the oscillating laser field to share energy with another electron during its collision with the residual ion. While the generally accepted mechanisms for NSDI are laser-induced recollision direct ionization (RDI) and recollision excitation with subsequent ionization (RESI) [3], NSDI can also take place through sequential ionization of doubly excited states that are populated after the laser-induced recollision [4].

The attractiveness of NSDI mainly originates from the fact that this phenomenon represents a uniquely clean example of electron-electron correlation enforced by an external field. The quest to understand electron-electron correlation in NSDI has greatly benefited from highly differential measurements. Since the groundbreaking experiment conducted 20 years ago, in which the correlated two-electron momentum distributions (CMDs) for NSDI of Ar were measured by Weber *et al.* [5], a number of kinematically complete measurements have been performed [3,6–8]. In the measurements of CMDs for NSDI, the data are integrated over the transverse momentum of the first and second electron such that only the parallel momentum

(the momentum component along the laser polarization axis) distributions are reported. The parallel momentum distributions for the correlated two-electron pair have been shown to be the most effective tool to investigate the underlying mechanisms of NSDI since they provide information that is much more detailed than the early measured momentum distributions and the total yields of the doubly charged ions in which many characteristic structures of that particular process are smoothed out. Generally, the measurements of CMDs for NSDI by linearly polarized laser light clearly show that the two electrons have a greater probability of being emitted in the same direction parallel to the laser polarization. However, at intensities below the recollision threshold, i.e., the minimum intensity required for the rescattering electron to have enough energy to ionize another electron in the parent ion, the measurements of CMDs for NSDI actually show an anticorrelation, indicating a significant probability for the electrons to drift out on opposite sides of the atom [9,10].

The observed anticorrelation in the experimental measurements [9,10] has attracted a large number of theoretical studies. However, the assignment of the observed anticorrelation to specific mechanisms still remains a challenge for theory. Based on classical or semiclassical models, multiple recollisions, in the context of RESI, were first put forth to explain anticorrelated two-electron escape [9,11,12]. However, other classical simulations disproved that multiple recollisions

cause the anticorrelated emission of the two electrons [13,14]. Instead, Coulomb repulsion between the two electrons was suggested as a possible mechanism [15]. Furthermore, while anticorrelation was also attributed to quantum tunneling in the semiclassical simulations [12], it was later argued that this effect does not matter in NSDI [16]. Recently another mechanism, Coulomb slingshot motion, was proposed by Katsoulis *et al.* [17] to explain anticorrelated two-electron escape. Using a three-dimensional semiclassical model, they also found that the anticorrelation pattern is more pronounced for shorter compared to longer pulses.

In addition to classical or semiclassical models, the S -matrix theory [18–20] has been employed to investigate the anticorrelated behavior. It was found that interference has a major influence on the shape, localization, and symmetry of the correlated electron momentum distributions [19]. However, it should be noted that although anticorrelation has been successfully predicted by the S -matrix theory when quantum interference between the contributions of different intermediate excited states has been incorporated, the obtained results have only qualitatively reproduced the experimental data. In fact, the simulated patterns of the correlated longitudinal momentum distributions were quite different from those observed experimentally [9,10].

While the abovementioned studies show that anticorrelation results from RESI, there also exist theoretical studies based on numerical solutions of the time-dependent Schrödinger equation (TDSE) [21] and the time-dependent Newton equation [22]. They show that anticorrelation can also be obtained through RDI.

The existing controversial debate on the mechanisms responsible for anticorrelation in NSDI clearly indicates that more theoretical studies are highly desirable. In the present work, we aim to investigate anticorrelation in NSDI of atoms driven by strong laser fields at intensities below the recollision threshold. We employ the recently improved quantitative rescattering (QRS) model, in which the lowering of the threshold due to the presence of the electric field at the instant of recollision is taken into account. The improved QRS model was first employed to evaluate the double-to-single ionization ratio for atoms in strong laser fields [23–25] and was later applied to CMD simulations for NSDI at intensities above the recollision threshold [26–28]. For the CMD calculations of NSDI below the threshold intensity, which is considered in the present paper, however, the QRS model needs to be improved further, since NSDI can only take place at recollision times when the barrier due to the combined external electric and internal Coulomb potential is sufficiently suppressed. Even though anticorrelation has only been observed experimentally in the measured CMD for NSDI of Ar, as a first step in this direction, we choose He as the target due to the fact that NSDI of the He atom serves as a prototype for exploring correlated electron dynamics in strong fields [7,8,11,15,17,29–34].

Unless specified otherwise, atomic units (a.u.) ($\hbar = |e| = m = 4\pi\epsilon_0 = 1$) are used throughout this paper.

II. THEORETICAL MODEL

While laser-induced rescattering processes can be qualitatively interpreted by the classical rescattering model [1,2], the

QRS approach provides a quantitative description. Based on the factorization formula in Refs. [35–37], the QRS model was first formulated for high-order above-threshold ionization [38] and high-order harmonic generation [39]. It was later extended to NSDI [40,41].

In this paper, we use the QRS model to calculate the CMD for NSDI of He at an intensity well below the recollision threshold. Since the contribution from RDI can be safely neglected for the case considered here, we only focus on the process of RESI in the present paper. Since the details of the improved QRS model for RESI have been presented in Refs. [27,42], we only give a brief review here with a description of the further improvements for anticorrelation.

According to the QRS model, the CMD of RESI for the momentum components p_1^{\parallel} and p_2^{\parallel} of the two outgoing electrons along the laser polarization direction can be expressed as a product of the parallel momentum distribution for the returning electron after recollision and the parallel momentum distribution for the electron tunnel-ionized from an excited state of the parent ion. This indicates that, in the QRS model, the laser-induced recollision excitation of the parent ion and the tunnel ionization of electrons from an excited state in RESI are disentangled and treated separately.

Electron impact excitation of the parent ion is described by employing a laser-free differential cross section (DCS) for this process. In the original QRS model, the incident energy is chosen as the kinetic energy that a returning electron accumulates in the laser field. This implies that the QRS model predicts no NSDI events when the maximum energy of the returning electron is less than the energy difference between the first excited state and the ground state of the parent ion. This clearly conflicts with the experimental observations at low intensities. This conflict, as argued by van der Hart and Burnett [43], arises from the assumption that laser-induced rescattering can be treated as if it takes place in a field-free atom or ion, where the total energy of a continuum electron must be positive. However, this is not necessarily the case when the collision takes place in an external electric field. Since the combined electric and atomic potentials form a barrier below zero, the incoming electron can escape from the atom or ion even with a negative total energy, provided that its energy is higher than the potential barrier after the collision. Therefore, the returning electron can donate more energy to the ionic electron compared to a laser-free collision. This is effectively equivalent to a lowering of the threshold, although the energy level of an excited state is not lowered.

Since it is still a formidable task to perform actual numerical calculations for recollision in the QRS model with the threshold lowering taken into account, a practical attempt is to adjust the collision energy [43]. For this purpose, it is assumed that the energy E_r of the laser-induced returning electron with respect to the maximum of the barrier in the combined atomic and electric field potentials at a recollision time t_r corresponds to the incoming electron energy E_i in the field-free case, i.e.,

$$E_i = E_r + \Delta E(t_r), \quad (1)$$

where $\Delta E(t_r)$ is the lowering of threshold (see Fig. 1 in Ref. [43]). For laser-induced recollision excitation,

$$\Delta E(t_r) = 2\sqrt{Z|F(t_r)|}, \quad (2)$$

where $Z(=1)$ is the asymptotic charge of the residual ion seen by the scattered electron, and $F(t_r)$ is the electric field at the recollision time.

To obtain the parallel momentum distribution for the returning electron after recollision, we first calculate the DCSs for laser-free electron impact excitation of He^+ . Here, we only need to consider the singlet DCSs since the two electrons involved in the laser-induced recollision process start in the singlet ground state of He and their singlet coupling is preserved [44]. Then we convert the scattering angle in the singlet DCS $d\sigma^s/d\Omega$ to the parallel momentum. Since the DCS is symmetric around the incident direction, the parallel momentum distribution for the scattered electron at the incident energy E_i is given by

$$Y_{E_i}(k_f^{\parallel}) = \frac{2\pi}{k_f} \frac{d\sigma^s}{d\Omega}, \quad (3)$$

where k_f is the momentum of the scattered electron, and $k_f^{\parallel} = k_f \cos \theta$, with θ being the scattering angle. The prefactor $2\pi/k_f$ in Eq. (3) is introduced to ensure

$$\int Y_{E_i}(k_f^{\parallel}) dk_f^{\parallel} = \int \frac{d\sigma^s}{d\Omega} d\Omega = \sigma^s. \quad (4)$$

Due to energy conservation, we have

$$E_i = \frac{1}{2}k_f^2 + I_p, \quad (5)$$

where I_p is the threshold energy for excitation. For the laser-induced recollision excitation taking place at t_r when the vector potential $A_r = A(t_r)$, the projectile electron is still under the influence of the laser field after the collision. As a result, it will gain an additional momentum $-A_r$ in the direction of the laser polarization from t_r to the end of the laser pulse. Finally, the corresponding parallel momentum distribution for the returning electron after recollision excitation in a strong field at an intensity I can be obtained from Eq. (3) by shifting the momentum of the projectile electron by $-A_r$, i.e.,

$$D_{E_i}^{\text{exc}}(p_1^{\parallel}) = Y_{E_i}(k_f^{\parallel} - A_r). \quad (6)$$

The vector potential A_r in Eq. (6) is related to the momentum $k_r (= \sqrt{2E_r})$ of the returning electron. In the QRS model, the relation between A_r and k_r is approximated by [38]

$$|A_r| = k_r/1.26. \quad (7)$$

To account for the lowering of the threshold, Eq. (7) should be rewritten as

$$|A_r| = \sqrt{2[E_i - \Delta E(t_r)]}/1.26. \quad (8)$$

The process of tunneling ionization of electron from the excited state of He^+ is described by solving the TDSE within the single-active-electron approximation [45]. Indeed, the Ammosov-Delone-Krainov (ADK) [46] model modified by Tong and Lin [47] is the simplest method that could be used to evaluate the parallel momentum distribution for tunneling ionization. However, since the shape of the parallel momentum distribution significantly depends on the ionization rate, but the ionization rate can hardly be predicted accurately by the ADK model, a much better choice is to solve the TDSE directly. In the present work, we first calculate the two-dimensional (2D) momentum distributions for

single ionization of electrons from excited states with a specified magnetic quantum number by solving the TDSE. Then the parallel momentum distributions for the tunnel-ionized electrons are obtained by integrating the 2D momentum distributions over the momentum components perpendicular to the laser polarization.

The prevalent view has been that rescattering occurs, most probably, near field crossings. However, for the case of low intensity in which the energy of the returning electron is smaller than the threshold energy for excitation, recollisions taking place near field crossings are unable to trigger NSDI. Therefore, one has to consider recollisions at the time after the field crossing when $E_r + \Delta E(t_r) > I_p$. Here, we assume that tunneling ionization begins immediately after recollision excitation. As is demonstrated in the next section, the initial tunneling ionization time plays an important role in the pattern of the parallel momentum distributions for electrons that are tunnel-ionized from excited states. To control the time at which tunneling ionization begins, we introduce a parameter t_r in the electric field used in the TDSE calculations,

$$\mathbf{F}(t) = a(t)F_0 \cos(\omega t + \phi) \hat{z}. \quad (9)$$

Here ω is the carrier frequency and ϕ the carrier envelope phase. The envelope function $a(t)$ is chosen to be constant for the first two cycles within $t_r \leq t \leq 2T$ and then ramped down over four cycles. Specifically,

$$a(t) = \begin{cases} 1 & (t_r \leq t \leq 2T); \\ \sin^2[\pi(6T - t)/(8T)] & (2T < t \leq 6T); \\ 0 & (t < t_r, t > 6T). \end{cases} \quad (10)$$

Here the returning time t_r is in the range of 0 to $T/4$, and the carrier envelope phase ϕ is set to $\pi/2$ to account for the recollision process in which the laser-induced recolliding electron returns to the origin along the $-\hat{z}$ direction. It should be noted that the parallel momentum distributions for electrons tunnel-ionized from excited states are obtained at the end of the laser pulse and the results remain essentially unchanged if a longer pulse with one or two more cycles is used.

With the parallel momentum distributions $D_{E_i}^{\text{exc}}(p_1^{\parallel})$ calculated by using Eq. (6) for excitation and $D_{t_r}^{\text{tun}}(p_2^{\parallel})$ calculated by solving the TDSE for tunneling ionization, the CMD for laser-induced electron impact excitation at the incident energy E_i with subsequent tunneling ionization in the laser field with a peak intensity I is obtained as

$$D_{E_i, t_r}(p_1^{\parallel}, p_2^{\parallel}) = D_{E_i}^{\text{exc}}(p_1^{\parallel}) \times D_{t_r}^{\text{tun}}(p_2^{\parallel}). \quad (11)$$

Note that $D_{t_r}^{\text{tun}}(p_2^{\parallel})$ depends on the recollision time t_r at which tunneling ionization begins. In addition, since excitation can always take place when $E_i \geq I_p$, an integral over E_i should be performed to account for the contributions from collisions at all incident energies. Therefore, the CMD for RESI at an intensity I is given by

$$D(p_1^{\parallel}, p_2^{\parallel}) = \int_{I_p}^{\infty} dE_i D_{E_i, t_r}(p_1^{\parallel}, p_2^{\parallel}) W(E_r), \quad (12)$$

where $E_r = E_i - \Delta E(t_r)$ and $W(E_r)$ is the recolliding wave packet (RWP) describing the energy (momentum) distribution of the returning (incoming) electron in the laser field [38]. The RWP can be calculated by using the second-order strong-field

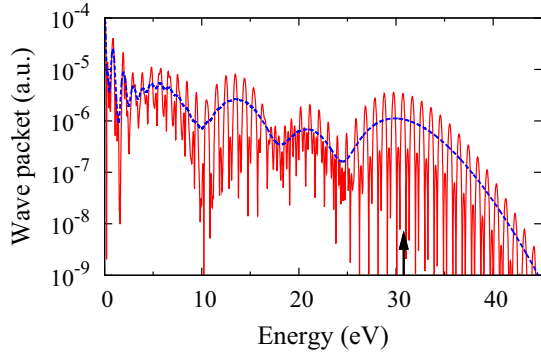


FIG. 1. Recolliding wave packet against the kinetic energy of the laser-induced returning electron in a 400-nm laser pulse with a peak intensity of 6.5×10^{14} W/cm². The blue broken curve is the smoothed wave packet used in the numerical calculations. The arrow indicates the cutoff at $3.17 U_p$.

approximation (SFA2) for HATI [38]. For He, the details of the RWP calculations were presented in Ref. [23].

III. RESULTS AND DISCUSSION

A. Calculations of correlated two-electron momentum distributions

We calculate the CMD of He atoms irradiated by few-cycle laser pulses with a wavelength of 400 nm and a peak intensity of 6.5×10^{14} W/cm².

According to the rescattering model, all the laser-induced rescattering processes are initiated by the collisions of the returning electrons with the parent ions. Therefore, the energy distribution of the returning electron in a laser field plays an essential role in the calculations. In the QRS model, the energy distribution of the returning electron is described by the RWP. Since all the rescattering processes share the same RWP, the RWP for NSDI can be extracted from the 2D momentum distribution for HATI due to elastic scattering of the returning electron with the parent ion. In Fig. 1 we show the obtained RWP as a function of the kinetic energy of the laser-induced returning electron. The electric field used in the calculations of the RWP is linearly polarized along the z axis and has a trapezoidal pulse shape with a four-cycle turn on, two cycles at full strength, and a four-cycle turn off. As shown in Fig. 1, a cutoff appears at $3.17 U_p = 31$ eV, corresponding to the maximum kinetic energy of the returning electron predicted by the classical rescattering model. This is well below the threshold energy for excitation of He⁺.

The energy distribution shown in Fig. 1 implies that one has to consider the potential change due to the presence of an electric field at the time of recollision. According to Eq. (2), the maximum value of this potential change is 20 eV for the laser pulse considered here. Consequently, RDI can be ruled out. To trigger RESI, the energy of the returning electron with respect to the barrier of the combined electric and atomic potentials must be higher than the excitation energy of the parent ion. Taking the maximum energy of the returning electron as 31 eV, only the *effective* recollisions taking place after a crossing of the driving field with “time delay” (i.e., the time difference between the recollision time and the time

at a crossing of the electric field) leading to ωt_r greater than 15° and 45° , when $\Delta E(t_r) = 10$ and 17 eV, can promote He⁺ from the ground state to the excited states with $n=2$ and $n=3$, respectively. However, it should be noted that the extension of the RWP beyond the cutoff indicates that the returning electron could possess higher energies, although with decreasing probabilities. Actually, it is the RWP, together with the time delay, that determines the weight of a contribution from recollision at a given incident energy.

In the actual numerical calculations of CMD, it is a tremendous challenge to consider all the effective recollisions possibly taking place at any time with $\omega t_r \geq 15^\circ$ (45°) for excitation to $n=2$ ($n=3$). Consequently, we choose an “average” recollision (returning) time to make the calculations tractable. An average recollision time was recently used successfully to account for the lowering of the potential due to the presence of an electric field at the instant of recollision in numerical simulations for the total yields of doubly charged ions [23–25], the CMDs for NSDI of atoms at intensities well above the recollision threshold [26,27], and the momentum distributions of doubly charged ions [48]. The method used to determine the average returning time was presented in detail in Ref. [26]. The average returning time is approximately given by

$$\bar{\theta}_r = \frac{\int_{\theta_1}^{\theta_2} \theta_r W_{\text{ADK}}(\theta_r) d\theta_r}{\int_{\theta_1}^{\theta_2} W_{\text{ADK}}(\theta_r) d\theta_r}, \quad (13)$$

where $\theta_r = \omega t_r$ and $W_{\text{ADK}}(\theta_r)$ is the ionization rate, obtained using the Ammosov-Delone-Krainov (ADK) model [46], for the electron that is ionized at time t_b and returns to the origin at time t_r . Here we neglect the Coulomb degeneracy of the He⁺ states [49,50].

Suppose an electron in the atom is released into a monochromatic laser field $\mathbf{F}(t) = \hat{z} F_0 \cos(\omega t)$, a one-to-one relation between the birth time t_b and the returning time t_r can be obtained by solving the one-dimensional (1D) Newton’s equation of motion for the system [38], i.e.,

$$\ddot{z}(t) = -F_0 \cos(\omega t). \quad (14)$$

Based on this 1D classical model, it was found that electrons born before $\omega t = 13^\circ$ will return at a time after $\omega t = 270^\circ$. According to the above analysis about the restricted effective recollision times, we choose $\theta_2 = 360^\circ$ and $\theta_1 = 285^\circ$ (315°) in Eq. (13) for excitation to $n=2$ ($n=3$). With these considerations, we obtain $\bar{\theta}_r \simeq 55^\circ$ and 70° after a crossing of the electric field for $n=2$ and 3, respectively.

To evaluate the parallel momentum distributions for the projectile electron after the laser-induced recollision, we first prepare the laser-free singlet DCSs for electron impact excitation of He⁺ from the ground state to the excited states of $n=2$ and $n=3$ for each angular momentum l with a specific magnetic quantum number m , respectively. Due to the n^{-3} scaling law, the contributions from higher excited states are neglected. [We use the short-hand notation $2p_0 \equiv 2p$ ($m=0$) and similarly for $2p_1$, $3p_0$, and $3p_1$]. By expressing the singlet DCSs as a function of the parallel momentum with the shift of the drift momentum taken into account, we obtain the parallel momentum distributions for the active electron after recolliding with the He⁺ ion. Figure 2 displays the results for

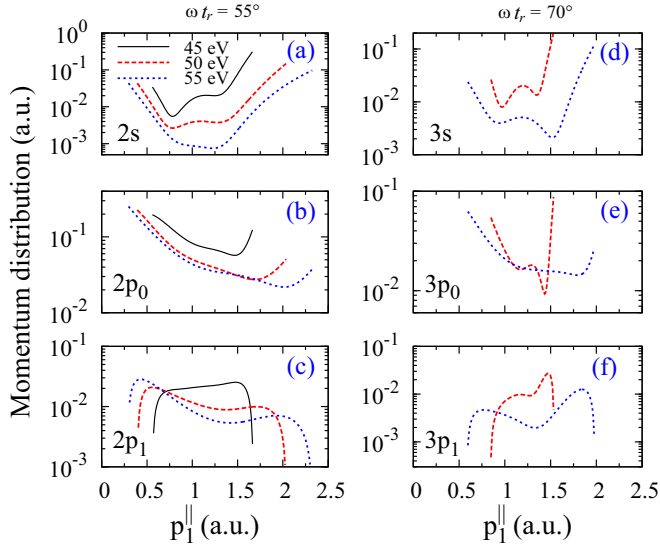


FIG. 2. Parallel momentum distributions for the active electron after recolliding with the He^+ ion and exciting the residual ground-state electron to the excited states of (a) $2s$, (b) $2p_0$, (c) $2p_1$, (d) $3s$, (e) $3p_0$, and (f) $3p_1$ in a 400-nm laser field with a peak intensity of $6.5 \times 10^{14} \text{ W/cm}^2$. The recolliding electron returns to the origin along the $-\hat{z}$ direction with energies of 45, 50, and 55 eV. The recollision times are chosen to be such that $\omega t_r = 55^\circ$ and 70° after a crossing of the electric field for $n=2$ and 3 , respectively.

exciting the residual ground-state electron to the excited states $2s$, $2p_0$, $2p_1$, $3s$, $3p_0$, and $3p_1$. According to the rescattering model, the final parallel momentum of the projectile electron that returns to the origin along the $-\hat{z}$ direction is restricted by [3]

$$-\sqrt{2(E_i - I_p)} - A_r \leq p_1^{\parallel} \leq \sqrt{2(E_i - I_p)} - A_r. \quad (15)$$

The above equation implies that the range of the momentum distribution shrinks for higher excited states. As demonstrated in Fig. 2, the momentum distributions for $n=3$ cover smaller ranges compared to those for $n=2$. In addition, it can be seen from Eqs. (7) and (8) that, with the lowering of the potential considered, the parallel momentum distributions shift to smaller momenta by

$$\Delta|A_r| = \{\sqrt{2E_i} - \sqrt{2[E_i - \Delta E(t_r)]}\}/1.26. \quad (16)$$

For example, $\Delta|A_r| = 0.31$ for $E_i = 50 \text{ eV}$ and $\omega t_r = 55^\circ$ for the laser field considered here.

Figure 3 displays the parallel momentum distributions for the tunnel-ionized electron from selected excited states of He^+ corresponding to those in Fig. 2. As mentioned before, these results were obtained by integrating the 2D momentum distributions from the TDSE over the momentum component perpendicular to the direction of the laser polarization. According to the classical rescattering model, the momentum of the tunneling electron is limited by $-A_0 \leq p_2^{\parallel} \leq A_0$, where A_0 is the maximum value of the vector potential. For the laser field considered here, $A_0 = 1.2$. Nevertheless, it can be seen from Fig. 3 that the parallel momentum distributions obtained from the TDSE clearly spread outside of A_0 . The most important feature of the momentum distributions is that they

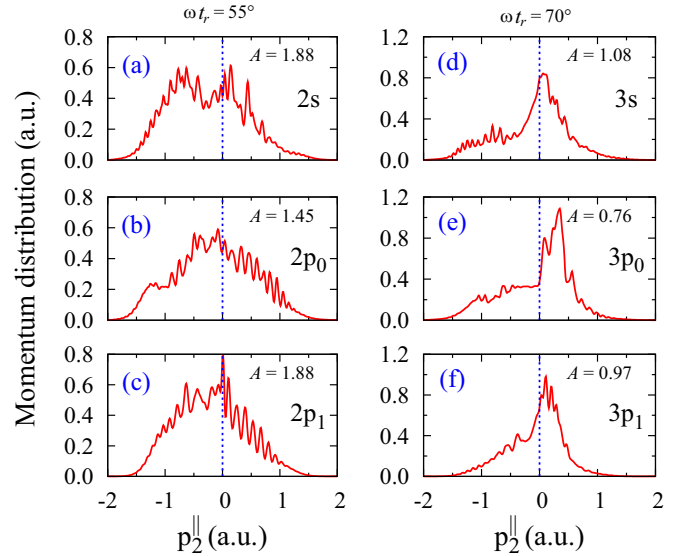


FIG. 3. Parallel momentum distributions for the electron ejected from He^+ in the excited states of (a) $2s$, (b) $2p_0$, (c) $2p_1$, (d) $3s$, (e) $3p_0$, and (f) $3p_1$ by a 400-nm laser field with a peak intensity of $6.5 \times 10^{14} \text{ W/cm}^2$. The recolliding electron returns to the origin along the $-\hat{z}$ direction at $\omega t_r = 55^\circ$ and 70° after a crossing of the electric field for $n=2$ and 3 , respectively. Asymmetry parameters for the momentum distributions are also indicated. See text for details.

are not symmetric with respect to $p_2^{\parallel} = 0$. The asymmetry of the momentum distribution can be represented by the parameter $A = P_L/P_R$, where P_L and P_R are the total single-ionization yields of electrons with negative and positive momenta, respectively. By integrating the distributions over the parallel momentum, we found that the asymmetry parameters are greater than 1 for $n=2$ but less than 1 for $n=3$, except for the case of $3s$ where the asymmetry parameter is slightly larger than 1. As is demonstrated below, the asymmetry of the momentum distribution for the electron being tunnel-ionized from an excited state of the singly charged ion plays a decisive role in forming the anticorrelated CMD.

With the recolliding wave packet evaluated within SFA2 and the parallel momentum distributions obtained from the R matrix and TDSE calculations for the two outgoing electrons, respectively, we are ready to calculate the CMDs for RESI using Eq. (12). The calculated correlated parallel momentum spectra for tunneling from the excited $2s$, $2p_0$, $2p_1$, $3s$, $3p_0$, and $3p_1$ states are displayed in Fig. 4. Note that in the CMDs presented in Fig. 4, the contributions from collisions by the laser-induced electron that returns to the parent ion along the direction of $-\hat{z}$ at all possible incident energies have been accounted for. As expected, the CMD for $2p_0$ dominates. Indeed, the patterns of the momentum distributions for the two outgoing electrons are both imprinted in the CMD. Since tunnel ionization does not depend on the returning electron energy, the distribution along p_2^{\parallel} in the CMD directly reflects the momentum distribution of the tunnel-ionized electron. The denser population in the region of $p_2^{\parallel} < 0$ for $n=2$ in Figs. 4(a)–4(c) results from the asymmetric distributions in Figs. 3(a)–3(c) with asymmetry parameters larger than 1. Similarly, the bright spots near $p_2^{\parallel} = 0$ for $n=3$

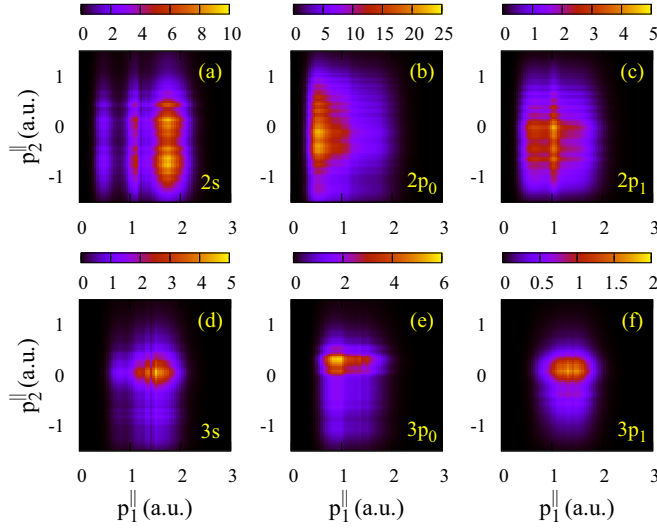


FIG. 4. Right-side ($p_1^{\parallel} > 0$) correlated parallel momentum spectra for excitation tunneling from (a) $2s$, (b) $2p_0$, (c) $2p_1$, (d) $3s$, (e) $3p_0$, and (f) $3p_1$ in a 400-nm laser field with a peak intensity of 6.5×10^{14} W/cm² with $\omega_r = 55^\circ$ and 70° for $n = 2$ and 3 , respectively.

in Figs. 4(d)–4(f) correspond to the sharp distributions in Figs. 3(d)–3(f).

According to the 1D classical model, if an electron is tunnel-ionized in a half cycle when the electric field is negative, it could be driven back to the parent ion along the $-\hat{z}$ direction. On the other hand, for a long pulse, if the electron is born during the other half cycle, it possesses the same probability for returning to the parent ion along the $+\hat{z}$ direction. Since $A(t \pm T/2) = -A(t)$, where $T = 2\pi/\omega$ denotes the field cycle, events whose times are displaced by half a cycle are related by momentum inversion. Furthermore, since both electrons are indistinguishable, the CMD for excitation + tunneling should be symmetric with respect to both diagonals, i.e., $p_1^{\parallel} = \pm p_2^{\parallel}$. However, it should be emphasized that the additional symmetry with respect to the coordinate axes, suggested by Feuerstein *et al.* [3], is never guaranteed. Figure 5 depicts the full-space CMDs for excitation + tunneling upon symmetrization of the CMDs displayed in Fig. 4. The CMDs for $2p_0$ and $2p_1$ reveal the dominance of back-to-back (anticorrelated) emission, whereas for $3p_0$ and $3p_1$ most populations are found close to the coordinate axes in quadrants 1 and 3, thus showing a distinct correlated behavior.

Figure 6(a) depicts the CMD for $n=2$ that consists of the distributions from $2s$, $2p_0$, and $2p_1$ (the latter result is multiplied by 2, since $2p_{-1}$ yields the same contribution as that of $2p_1$). Due to the dominance of $2p_0$, the CMD for $n=2$ is reminiscent of that for $2p_0$. Similarly, the result for $n=3$ is shown in Fig. 6(b). Finally, by summing the CMDs in Figs. 6(a) and 6(b), we obtain the CMD for excitation tunneling from all excited states with $n=2$ and 3. As displayed in Fig. 6(c), it exhibits a strong anticorrelated emission. The present final CMD for RESI of He is found to be in good agreement with the simulated result from a classical ensemble model [15] in which the same laser parameters

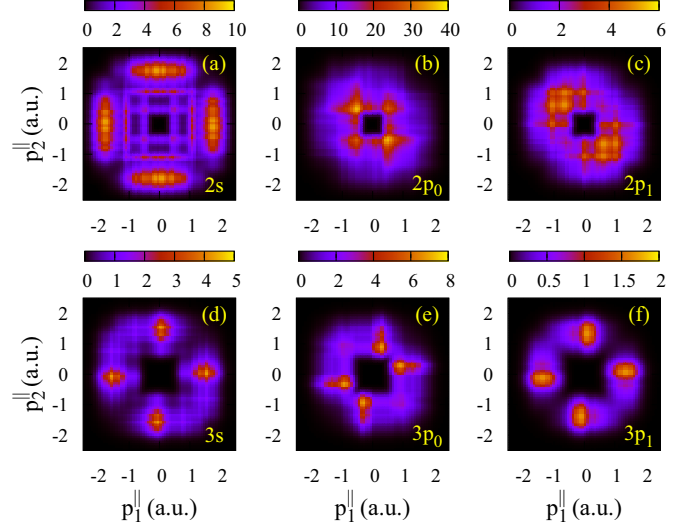


FIG. 5. Symmetrized full-space correlated parallel momentum spectra for excitation tunneling from the excited states of (a) $2s$, (b) $2p_0$, (c) $2p_1$, (d) $3s$, (e) $3p_0$, and (f) $3p_1$ in a 400-nm laser field with a peak intensity of 6.5×10^{14} W/cm².

were used. Very recently, by employing a three-dimensional semiclassical model, Katsoulis *et al.* [17] also calculated the CMD for NSDI of He in a laser pulse at 400 nm but with a lower peak intensity of 5×10^{14} W/cm². As demonstrated in Ref. [17], at this lower intensity, the two electrons escape overwhelmingly in opposite directions, thus showing a strong anticorrelation.

We note that the present model predicts no events for small momenta in the center of the CMD. This is different from existing classical simulations [15,17] in which the populations also appear around zero momenta for two electrons, albeit with very small intensities. The empty population in the center of the CMD in Fig. 6 is due to the fact that only an averaged collision time is used in the present calculations. From Eqs. (8) and (15), one can see that the range of the momentum distribution for the laser-induced returning electron after collision depends on the recollision time. Consequently, the small-momenta region in the center of the CMD would be populated if all possible recollision times were considered.

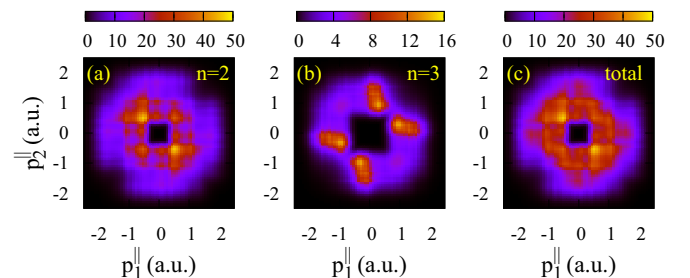


FIG. 6. Correlated parallel momentum spectra for excitation tunneling from all possible excited states of (a) $n=2$, (b) $n=3$, and (c) sum of $n=2$ and 3 in a 400-nm laser field with a peak intensity of 6.5×10^{14} W/cm².

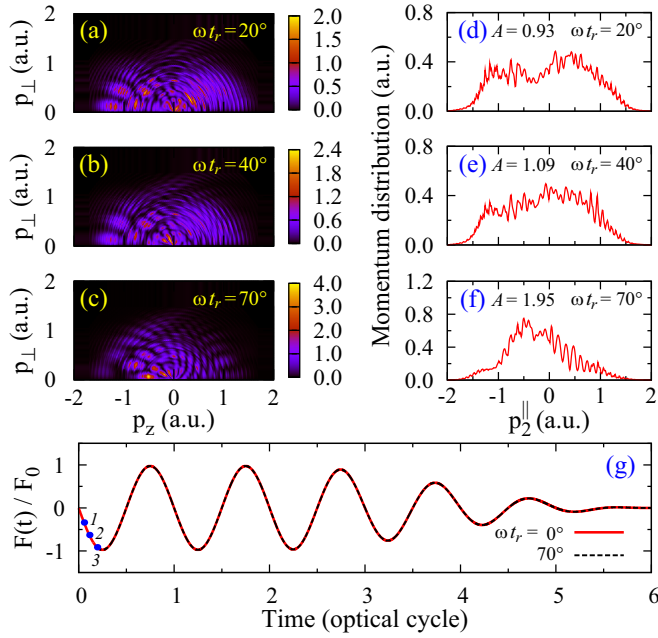


FIG. 7. (a, b, c) Two-dimensional photoelectron momentum distributions parallel (p_{\parallel}) and perpendicular ($p_{\perp} = \sqrt{p_x^2 + p_y^2}$) to the laser polarization direction from the TDSE for single ionization of He^+ from the excited $2p_0$ state in a 400-nm laser field with a peak intensity of $6.5 \times 10^{14} \text{ W/cm}^2$. (d, e, f) Parallel momentum distributions for the ionized electron obtained from panels (a), (b), and (c), respectively. (g) Electric fields used in the TDSE calculations with the beginning times of $\omega t_r = 20^\circ$, 40° , and 70° marked by points 1, 2, and 3, respectively. The red solid and black dotted lines represent the electric fields with $\omega t_r = 0^\circ$ and 70° , respectively.

B. Interpretation of mechanism for anticorrelation

We start by showing how the recollision time alters the distribution of tunnel-ionized electrons in the TDSE calculations. Figure 7 displays the 2D photoelectron momentum distributions parallel ($p_{\parallel} = p_z$) and perpendicular ($p_{\perp} = \sqrt{p_x^2 + p_y^2}$) to the laser polarization direction from the TDSE for single ionization of He^+ from the excited $2p_0$ state, the corresponding parallel momentum distributions, and the laser fields used in the TDSE calculations. One can see from Figs. 7(a)–7(c) that, while all the 2D momentum spectra reveal typical features, such as a fanlike structure at low energies and circular rings at high energies, for above-threshold ionization, the left-side ($p_z < 0$) distribution becomes denser as the initial ionization time increases. As a result, the asymmetry parameters for the parallel momentum distributions shown in Figs. 7(d)–7(f) increase accordingly. As is discussed below, this trend is of great importance in leading to anticorrelation.

Although solving the TDSE provides accurate numerical results, insight into the underlying physics is hidden. To unveil the role of the recollision time (initial ionization time) in the momentum distribution of the tunnel-ionized electron, we employ the ADK model [46], which provides an intuitive interpretation of the tunnel-ionization process. With the depletion effect taken into account, the ADK rate can be expressed as

$$Y^{\text{ADK}}(t) = W[|F(t)|]e^{-\int_{t_r}^t W[|F(t')|]dt'}, \quad (17)$$

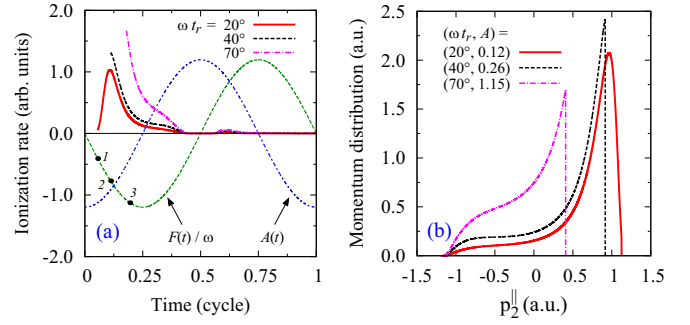


FIG. 8. (a) ADK rate for ionization of He^+ from $2p_0$ vs time in a 400-nm laser field with a peak intensity of $6.5 \times 10^{14} \text{ W/cm}^2$ with initial ionization times corresponding to $\omega t_r = 20^\circ$, 40° , and 80° , respectively. The electric field and vector potential of the laser field are also plotted. In the electric field the initial ionization times corresponding to $\omega t_r = 20^\circ$, 40° , and 80° are marked by points 1, 2, and 3, respectively. (b) Parallel momentum distributions of the ionized electron corresponding to the ADK rates shown in panel (a). The asymmetry parameters are also indicated.

where $W[|F(t)|]$ is the modified ADK rate given by Eq. (2) in Ref. [47]. Note that the integral of $Y^{\text{ADK}}(t)$ over time yields the total ionization probability, i.e.,

$$P = \int_{t_r}^t Y^{\text{ADK}}(t)dt = 1 - e^{-\int_{t_r}^t W[|F(t')|]dt'}. \quad (18)$$

In Fig. 8(a), we show the ionization rate $Y^{\text{ADK}}(t)$ of He^+ from $2p_0$ in a 400-nm laser field with a peak intensity of $6.5 \times 10^{14} \text{ W/cm}^2$ with initial ionization times at $\omega t_r = 20^\circ$, 40° , and 80° , respectively. One can see that all the excited atomic ions are ionized within an optical cycle in the subsequent strong laser field even with different initial ionization times.

The momentum spectra of the excited electron after tunnel ionization at the end of the laser pulse are obtained by shifting the initial momentum by the drift momentum, which is the vector potential at the time the electron is ionized. Assuming that the electron is tunnel-ionized with zero initial velocity, the momentum spectrum is given by

$$D^{\text{ADK}}(p_{\parallel}^{\parallel}) = D^{\text{ADK}}[-A(t)] = \frac{1}{|E(t)|} Y^{\text{ADK}}(t). \quad (19)$$

Using Eq. (19), we calculated the parallel momentum distributions corresponding to the ADK rates shown in Fig. 8(a). The results are displayed in Fig. 8(b). At first glance, the momentum spectra calculated by using the ADK model in Fig. 8(b) are quite different from those evaluated by solving the TDSE in Figs. 7(d)–7(f). First, while the momentum spectra from the TDSE extend beyond the range of $[-A_0, A_0]$, the momentum of the tunneling electron in the ADK model is completely limited by $-A_0 \leq p_{\parallel}^{\parallel} \leq -A(t_r)$, where $A(t_r)$ is the vector potential at the initial tunneling time t_r . Consequently, the ADK distribution on the right side is squeezed towards smaller momenta as the initial tunneling time increases. Second, the sharp peak on the right side at the end of momentum distribution predicted by ADK is not observed in the corresponding TDSE results. This difference clearly indicates that the ADK model is unable to produce reliable parallel momentum spectra for tunnel-ionized electrons involved in

RESI, at least not for the situations considered here. The high peak in the momentum distributions is due to the fact that the ADK model significantly overestimates the ionization rates.

Despite the distinct discrepancies between the parallel momentum distributions from the ADK model and the TDSE, both exhibit a clear trend towards increasing asymmetry parameters with increasing initial ionization time. Below, we analyze in detail the reason for this trend.

According to Eq. (19), the ADK rates for ionization before (after) $T/4$ with $A(t) < 0$ [$A(t) > 0$] result in momentum distributions with $p_2^{\parallel} > 0$ ($p_2^{\parallel} < 0$). For a monochromatic laser field shown in Fig. 8(a), the ADK rate as a function of time without taking into account depletion is symmetric with respect to the peak of laser field within each of a half cycle. However, once the depletion effect can no longer be neglected, the ionization rate at $T/4 + t$ is always smaller than that at $T/4 - t$. Therefore, the symmetry is broken and asymmetric momentum distributions with $A < 1$ are generated if the initial ionization time is chosen to be $\omega t_r = 0$. However, as the initial ionization time increases, the total yield before the laser field reaches its maximum value at $T/4$ decreases. As a result, the asymmetry parameter for the parallel momentum distributions increases. As seen in Fig. 8, once the initial ionization time is sufficiently “delayed,” the asymmetry parameter for the momentum distribution becomes greater than 1, which is referred to as “antisymmetric” in the present paper.

We emphasize that the ADK model was only employed here to analyze the trend of the asymmetry in the parallel momentum distributions generated by solving the TDSE shown in Figs. 7(d)–7(f). It was never adopted in the numerical calculations for the CMD in this work, since for the tunneling ionization considered here, the excited states of He^+ require special treatment due to the Coulomb degeneracy [49,50].

Next, we show that only with the “antisymmetric” ($A > 1$) momentum distributions of the tunnel-ionized electron can an anticorrelated CMD be formed. For this purpose, we first display in Figs. 9(a)–9(c) the right-side ($p_1^{\parallel} > 0$) CMD for excitation tunneling from $2p_0$ in a 400-nm laser field with a peak intensity of $6.5 \times 10^{14} \text{ W/cm}^2$ with $\omega t_r = 20^\circ$, 40° , and 70° , respectively. Here, for simplicity, we only choose $E_i = 45 \text{ eV}$. Therefore, all the CMDs in Figs. 9(a)–9(c) share the same distribution along p_1^{\parallel} , except that, as the initial ionization time increases, the spectra move towards $p_1^{\parallel} = 0$ due to the increasing potential change. On the other hand, the momentum distributions depicted in Figs. 9(a)–9(c) along p_2^{\parallel} are different. They completely reflect the parallel momentum distributions for the tunneling ionized electron displayed in Figs. 7(d)–7(f), respectively. The asymmetry parameters for the parallel momentum distributions in Figs. 7(d) and 7(e) are both close to 1, but with a small change from less than 1 to greater than 1. On the other hand, as the initial time increases further, the parallel momentum distributions in Fig. 7(f) become highly asymmetric with a large asymmetry parameter close to 2.

The change of the asymmetry parameter from less than 1 to greater than 1 leads to the transition of RESI from (positively) correlated to anticorrelated electron emission. This is demonstrated in Figs. 9(d)–9(f), which display the symmetrized full-space CMDs obtained from Figs. 9(a)–9(c), respectively.

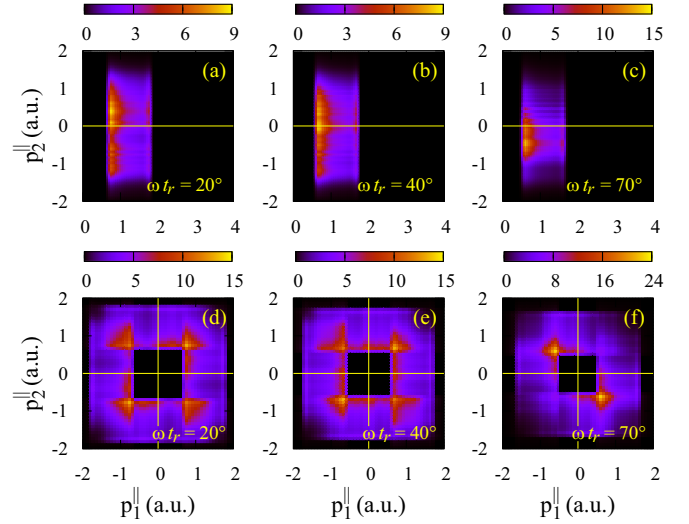


FIG. 9. (a, b, c) Right-side ($p_1^{\parallel} > 0$) correlated parallel momentum spectra for excitation tunneling from $2p_0$ in a 400-nm laser field with a peak intensity of $6.5 \times 10^{14} \text{ W/cm}^2$ for $E_i = 45 \text{ eV}$ and $\omega t_r = 20^\circ$, 40° , and 70° , respectively. (d, e, f) Symmetrized full-space correlated parallel momentum spectra obtained from panels (a), (b), and (c), respectively.

The ratio of the total yield in the fourth (second) quadrant to that in the first (third) quadrant in the symmetrized full-space CMD is the same as the ratio of the total yield in the region below $p_2^{\parallel} = 0$ to that in the region above $p_2^{\parallel} = 0$ in the corresponding right-side CMD. Furthermore, this is just the asymmetry parameter for the parallel momentum distributions of the tunnel-ionized electron. This is the reason why the CMD in Fig. 7(f) exhibits a strong anticorrelated behavior.

It should be noted that, in the QRS model, the laser-induced electron is assumed to be ejected immediately after recollision. Then, according to the above analysis based on the ADK model, if the recollision takes place at a time before the field reaches a maximum and the excited electron ionizes after the field maximum or just before the field reaches a maximum again, the two electrons escape into opposite hemispheres. Otherwise, if the two electrons are both ionized before the field maximum, they move into the same hemisphere. This argument is consistent with that made by Zhou *et al.* [15] in the context of a trajectory analysis based on their classical model.

Although the mechanism for anticorrelation has now been clearly unveiled, there still exist two issues that have not been addressed. (i) Why does the CMD for $n=3$ displayed in Fig. 6(b) show a (positively) correlated rather than an anticorrelated distribution? (ii) Why does the anticorrelation disappear at high laser intensities? To answer these questions, we again consider the ionization rate. It is well known that the ionization rate depends strongly on both the ionization potential and the intensity of the laser field. Since the ionization potential for $n=3$ is smaller than that for $n=2$, tunneling ionization occurs much faster, such that the total yield for single ionization during the time interval $[\omega t_r, T/4]$ could be larger than that in the subsequent time interval $[T/4, T/2]$. This explains why, even with a larger initial ionization time,

the asymmetry parameters for the parallel momentum distributions of tunnel-ionized electrons from $3s$, $3p_0$, and $3p_1$ are much smaller than the corresponding ones for the cases of $2s$, $2p_0$, and $2p_1$, as demonstrated in Fig. 3. Interestingly, Figs. 8(b) and 3(e) show that the sharp peak near zero momentum in the parallel momentum distributions for tunnel-ionized electrons from $2p_0$ with $\omega t_r = 80^\circ$ obtained from the ADK model is similar to that in the distributions for $3p_0$ evaluated by solving the TDSE. This confirms again that the ADK model overestimates the ionization rates significantly.

The absence of anticorrelation in the CMD for RESI at high intensities is also attributed to the rapidly increased ionization rate. Furthermore, it should be noted that, at high intensities, recollisions at any time could lead to RESI. Therefore, the average returning time is smaller (earlier) than that at low intensities. As a result, the total yield for single ionization during the time interval $[\omega t_r, T/4]$ is always larger than that in the subsequent time interval $[T/4, T/2]$. Besides, for NSDI at intensities in the regime above the recollision threshold, substantial contributions from RDI will cause additional enhancement of the probability for electron pairs being emitted in the same direction parallel to the laser polarization.

IV. CONCLUSIONS

Using the improved QRS model, we have calculated the correlated two-electron momentum distributions for NSDI of helium in a 400-nm laser pulse at an intensity well below the recollision threshold. Since the maximum energy of the laser-induced returning electron (the first electron), according to the classical rescattering model, is not sufficient to promote the parent ion to its first excited state, the lowering of the threshold due to the presence of an electric field at the instant of recollision has to be considered. To account for this effect in the numerical calculations, we used an average (returning) recollision time less than $T/4$ after a crossing of the driving field. Other than that, all our theoretical treatments

are based on accurate, fully quantum mechanical calculations. The present model predicts a distinct anticorrelation pattern in the correlated two-electron momentum distributions, which is in accord with existing theoretical results obtained from (semi)classical models [15,17].

In contrast to previous studies, however, our investigation reveals that it is the antisymmetric parallel momentum distribution of the tunnel-ionized electron (the second electron) that leads to the dominance of anticorrelated emission. We found that the antisymmetry of the parallel momentum distribution for the tunnel-ionized electron is caused by a “delayed” recollision time. The recollision time is forced to be delayed due to the fact that, only when the barrier of the Coulomb potential is suppressed by a sufficiently large electric field at the instant of recollision, can the laser-induced returning electron donate enough energy to the ionic electron to be excited. While the “delayed” recollision time predominantly determines the parallel momentum distribution of the tunneling electron and plays a decisive role in forming anticorrelation, the intensity and the wavelength of the laser field as well as the ionization potential of the excited state from which the electron is tunnel-ionized are additional quantities of high significance in anticorrelated emission. The present work, therefore, provides a reasonable explanation of the mechanisms leading to both anticorrelated and (positively) correlated two-electron escape in NSDI.

ACKNOWLEDGMENTS

This work was supported by the National Natural Science Foundation of China under Grants No. 11274219 and No. 11874246 and by the Guangdong Basic and Applied Basic Research Foundation under Grant No. 2021A1515010047. T.M. was supported in part by the Japan Society for the Promotion of Science under Grant No. 19H00887. O.Z. and K.B. were supported by the U.S. National Science Foundation under Grants No. PHY-1803844 and No. OAC-1834740, as well as the XSEDE Allocation No. PHY-090031.

- [1] K. J. Schafer, B. Yang, L. F. DiMauro, and K. C. Kulander, *Phys. Rev. Lett.* **70**, 1599 (1993).
- [2] P. B. Corkum, *Phys. Rev. Lett.* **71**, 1994 (1993).
- [3] B. Feuerstein, R. Moshhammer, D. Fischer, A. Dorn, C. D. Schröter, J. Deipenwisch, J. R. Crespo Lopez-Urrutia, C. Höhr, P. Neumayer, J. Ullrich, H. Rottke, C. Trump, M. Wittmann, G. Korn, and W. Sandner, *Phys. Rev. Lett.* **87**, 043003 (2001).
- [4] Y. Liu, L. Fu, D. Ye, J. Liu, M. Li, C. Wu, Q. Gong, R. Moshhammer, and J. Ullrich, *Phys. Rev. Lett.* **112**, 013003 (2014).
- [5] T. Weber, H. Giessen, M. Weckenbrock, G. Urbasch, A. Staudte, L. Spielberger, O. Jagutzki, V. Mergel, M. Vollmer, and R. Dörner, *Nature (London)* **405**, 658 (2000).
- [6] M. Weckenbrock, D. Zeidler, A. Staudte, T. Weber, M. Schöffler, M. Meckel, S. Kammer, M. Smolarski, O. Jagutzki, V. R. Bhardwaj, D. M. Rayner, D. M. Villeneuve, P. B. Corkum, and R. Dörner, *Phys. Rev. Lett.* **92**, 213002 (2004).
- [7] A. Staudte, C. Ruiz, M. Schöffler, S. Schössler, D. Zeidler, Th. Weber, M. Meckel, D. M. Villeneuve, P. B. Corkum, A. Becker, and R. Dörner, *Phys. Rev. Lett.* **99**, 263002 (2007).
- [8] A. Rudenko, V. L. B. de Jesus, Th. Ergler, K. Zrost, B. Feuerstein, C. D. Schröter, R. Moshhammer, and J. Ullrich, *Phys. Rev. Lett.* **99**, 263003 (2007).
- [9] Y. Liu, S. Tschuch, A. Rudenko, M. Dürr, M. Siegel, U. Morgner, R. Moshhammer, and J. Ullrich, *Phys. Rev. Lett.* **101**, 053001 (2008).
- [10] Y. Liu, D. Ye, J. Liu, A. Rudenko, S. Tschuch, M. Dürr, M. Siegel, U. Morgner, Q. Gong, R. Moshhammer, and J. Ullrich, *Phys. Rev. Lett.* **104**, 173002 (2010).
- [11] S. L. Haan, Z. S. Smith, K. N. Shomsky, and P. W. Plantinga, *J. Phys. B* **41**, 211002 (2008).
- [12] D. F. Ye and J. Liu, *Phys. Rev. A* **81**, 043402 (2010).
- [13] X. Ma, Y. Zhou, and P. Lu, *Phys. Rev. A* **93**, 013425 (2016).
- [14] S. Dong, X. Chen, J. Zhang, and X. Ren, *Phys. Rev. A* **93**, 053410 (2016).
- [15] Y. Zhou, C. Huang, and P. Lu, *Phys. Rev. A* **84**, 023405 (2011).

- [16] Z. L. Zhang, L. H. Bai, and J. T. Zhang, *Phys. Rev. A* **90**, 023410 (2014).
- [17] G. P. Katsoulis, A. Hadjipittas, B. Bergues, M. F. Kling, and A. Emmanouilidou, *Phys. Rev. Lett.* **121**, 263203 (2018).
- [18] X. L. Hao, J. Chen, W. D. Li, B. Wang, X. Wang, and W. Becker, *Phys. Rev. Lett.* **112**, 073002 (2014).
- [19] A. S. Maxwell and C. Figueira de Morisson Faria, *Phys. Rev. A* **92**, 023421 (2015).
- [20] A. S. Maxwell and C. Figueira de Morisson Faria, *Phys. Rev. Lett.* **116**, 143001 (2016).
- [21] D. I. Bondar, G. L. Yudin, W.-K. Liu, M. Yu. Ivanov, and A. D. Bandrauk, *Phys. Rev. A* **83**, 013420 (2011).
- [22] Z. Zhang, J. Zhang, L. Bai, and X. Wang, *Opt. Express* **23**, 7044 (2015).
- [23] Z. Chen, Y. Zheng, W. Yang, X. Song, J. Xu, L. F. DiMauro, O. Zatsarinny, K. Bartschat, T. Morishita, S.-F. Zhao, and C. D. Lin, *Phys. Rev. A* **92**, 063427 (2015).
- [24] Z. Chen, X. Li, O. Zatsarinny, K. Bartschat, and C. D. Lin, *Phys. Rev. A* **97**, 013425 (2018).
- [25] Z. Chen, L. Zhang, Y. Wang, O. Zatsarinny, K. Bartschat, T. Morishita, and C. D. Lin, *Phys. Rev. A* **99**, 043408 (2019).
- [26] Z. Chen, Y. Wang, L. Zhang, and X. Jia, *Phys. Rev. A* **99**, 033401 (2019).
- [27] Z. Chen, Y. Wang, T. Morishita, X. Hao, J. Chen, O. Zatsarinny, and K. Bartschat, *Phys. Rev. A* **100**, 023405 (2019).
- [28] Z. Cheng, F. Liu, H. Wen, T. Morishita, O. Zatsarinny, and K. Bartschat, *Opt. Express* **28**, 22231 (2020).
- [29] J. S. Parker, B. J. S. Doherty, K. T. Taylor, K. D. Schultz, C. I. Blaga, and L. F. DiMauro, *Phys. Rev. Lett.* **96**, 133001 (2006).
- [30] A. Becker, R. Dörner, and R. Moshhammer, *J. Phys. B* **38**, S753 (2005).
- [31] K. T. Taylor, J. S. Parker, D. Dundas, and K. J. Meharg, *J. Mod. Opt.* **54**, 1959 (2007).
- [32] A. Emmanouilidou, J. S. Parker, L. R. Moore, and K. T. Taylor, *New J. Phys.* **13**, 043001 (2011).
- [33] K. Henrichs, S. Eckart, A. Hartung, D. Trabert, K. Fehre, J. Rist, H. Sann, M. Pitzer, M. Richter, H. Kang, M. S. Schöffler, M. Kunitski, T. Jahnke, and R. Dörner, *Phys. Rev. A* **98**, 043405 (2018).
- [34] J. Zhu and A. Scrinzi, *Phys. Rev. A* **101**, 063407 (2020).
- [35] T. Morishita, A.-T. Le, Z. Chen, and C. D. Lin, *Phys. Rev. Lett.* **100**, 013903 (2008).
- [36] T. Morishita and O. I. Tolstikhin, *Phys. Rev. A* **96**, 053416 (2017).
- [37] Y. Okajima, O. I. Tolstikhin, and T. Morishita, *Phys. Rev. A* **85**, 063406 (2012).
- [38] Z. Chen, A.-T. Le, T. Morishita, and C. D. Lin, *Phys. Rev. A* **79**, 033409 (2009).
- [39] A.-T. Le, R. R. Lucchese, S. Tonzani, T. Morishita, and C. D. Lin, *Phys. Rev. A* **80**, 013401 (2009).
- [40] Z. Chen, Y. Liang, and C. D. Lin, *Phys. Rev. A* **82**, 063417 (2010).
- [41] Z. Chen, Y. Liang, D. H. Madison, and C. D. Lin, *Phys. Rev. A* **84**, 023414 (2011).
- [42] Z. Chen, F. Liu, and H. Wen, *Chin. Phys. B* **28**, 123401 (2019).
- [43] H. W. van der Hart and K. Burnett, *Phys. Rev. A* **62**, 013407 (2000).
- [44] G. L. Yudin and M. Yu. Ivanov, *Phys. Rev. A* **64**, 035401 (2001).
- [45] T. Morishita, Z. Chen, S. Watanabe, and C. D. Lin, *Phys. Rev. A* **75**, 023407 (2007).
- [46] M. V. Ammosov, N. B. Delone, and V. P. Krainov, *Zh. Eksp. Teor. Fiz.* **91**, 2008 (1986).
- [47] X. M. Tong and C. D. Lin, *J. Phys. B* **38**, 2593 (2005).
- [48] C. Jia, P. Zhang, H. Wen, and Z. Chen, *Chin. Phys. B* **30**, 023401 (2021).
- [49] T. Yamabe, A. Tachibana, and H. J. Silverstone, *Phys. Rev. A* **16**, 877 (1977).
- [50] P. K. Samygin, T. Morishita, and O. I. Tolstikhin, *Phys. Rev. A* **98**, 033401 (2018).